Available online at www.sciencedirect.com

SciVerse ScienceDirect

Ceramics International 39 (2013) 3371–3375

CERAMICS INTERNATIONAL

www.elsevier.com/locate/ceramint

Short communication

Chitosan-assisted combustion synthesis of CuO–ZnO nanocomposites: Effect of pH and chitosan concentration

Thongthai Witoon[a,b,*], Tinnavat Permsirivanich[a], Metta Chareonpanich[a,b]

[a]*National Center of Excellence for Petroleum, Petrochemicals and Advance Material, Department of Chemical Engineering, Faculty of Engineering, Kasetsart University, Bangkok 10900, Thailand*

[b]*Center for Advanced Studies in Nanotechnology and Its Applications in Chemical Food and Agricultural Industries, Kasetsart University, Bangkok 10900, Thailand*

Received 8 June 2012; received in revised form 7 August 2012; accepted 8 August 2012
Available online 19 August 2012

Abstract

CuO–ZnO nanocomposites were synthesized via a chitosan-assisted solution combustion method. The effects of pH and chitosan concentration on the physicochemical properties of the CuO–ZnO nanocomposites have been investigated. Thermal behavior, morphological structures, surface composition, crystal type and specific surface area of the products were characterized by means of thermal gravimetric and differential temperature analysis, scanning electron microscopy, energy dispersive X-ray spectroscopy, X-ray diffraction and N_2-sorption analysis, respectively. Without the use of chitosan, CuO and ZnO particles were separately formed while CuO and ZnO crystallite sizes tended to be decreased with increasing the pH value. Chitosan was found to not only induce a homogeneous mixture of CuO–ZnO nanocomposites but also prevent the growth of CuO and ZnO nanoparticles. Moreover, chitosan also acted as a fuel which promoted the formation of CuO and ZnO nanoparticles at lower temperature.

Keywords: B. Composites; Chitosan; Solution combustion

1. Introduction

Nanocomposites are of great interest in many scientific and technological disciplines as they not only provide the best properties of their individual parents but also create the considerable synergy effects. Recently, CuO–ZnO nanocomposites have received much attention due to their potential uses in many applications, such as catalyst for methanol synthesis [1], solar cells [2], gas sensors [3,4] and photocatalysis [5,6]. Taking photocatalysis as an example, the composites of ZnO and CuO were found to reduce the recombination of electrons and holes and thus promoted the photocatalytic activity to be more efficient than that of an individual ZnO [5,6].

Various techniques such as hydrothermal [4], co-precipitation [7], sol–gel [8] and solution combustion [9–13] have been used to prepare metal oxide nanocomposites. Among these, the solution combustion, a redox reaction taken place between an oxidant and a fuel, has a great advantage through relative low temperature and simple equipment, which makes this method suitable and economic for large-scale production. Several organic compounds such as glycine [9], citric acid [10,11], urea [10,12], L-alanine [10] and polyethylene glycol [13] were found to not only act as a fuel but also have a significant influence in a nucleation and growth of the primary nanoparticles, resulting in a variety of size, shape, phase composition, morphology as well as their potential application [14]. In addition to organic compound, the synthesis parameters such as pH and temperature of the solution considerably affected the variation in the type of metal species [15,16] as well as the structural configuration of the organic compounds [17].

Chitosan, which is a non-toxic, inexpensive and bio-compatible polymer, is an interesting material to be used as

*Corresponding author at: National Center of Excellence for Petroleum, Petrochemicals and Advance Material, Department of Chemical Engineering, Faculty of Engineering, Kasetsart University, Bangkok 10900, Thailand. Tel.: +66 2579 2083; fax: +66 2561 4621.
E-mail address: fengttwi@ku.ac.th (T. Witoon).

0272-8842/$ - see front matter © 2012 Elsevier Ltd and Techna Group S.r.l. All rights reserved.
http://dx.doi.org/10.1016/j.ceramint.2012.08.018

a fuel in the synthesis of metal oxide nanocomposites since a large number of active hydroxyl and amine groups along the backbone chains of chitosan molecules can serve as coordination sites. Herein we propose a novel and promising bioploymer, chitosan, as an organic additive for the solution combustion synthesis of CuO–ZnO nanocomposites. The effects of pH and chitosan concentration on combustion characteristics and physical properties of the composites were investigated and characterized by means of thermal gravimetric and differential thermal analysis (TG–DTA), N_2-sorption isotherms, X-ray diffraction (XRD) and scanning electron microscopy (SEM).

2. Experimental

2.1. Chemicals and reagents

Copper nitrate trihydrate $Cu(NO_3)_2 \cdot 3H_2O$, zinc nitrate hexahydrate $Zn(NO_3)_2 \cdot 6H_2O$, acetic acid CH_3COOH and ammonium hydroxide NH_4OH (28 wt%) were purchased from Sigma-Aldrich Company. Chitosan with 80% deacetylation was purchased from Eland Corporation. The molecular weight of the chitosan determined by Gel Permeation Chromatography (GPC, Waters 600E) using 0.5 M acetic acid and 0.5 M sodium acetate as the eluent was found to be approximately 290 kDa. All chemicals and reagents are of analytical grade and used without any further purification.

2.2. Preparation of CuO–ZnO nanocomposites

Chitosan was dissolved overnight in 100 mL of 1% v/v acetic acid in deionized water at room temperature, agitated with a magnetic stirrer. Subsequently, 3.749 g $Cu(NO_3)_2 \cdot 3H_2O$ and 4.616 g $Zn(NO_3)_2 \cdot 6H_2O$ (mole ratio of Cu/Zn = 1/1) were added into the chitosan solution. Then the pH value of the mixture was quickly adjusted to 6 by the addition of aqueous NH_4OH. The resulting mixture was stirred at 333 K for 6 h to ensure the chitosan completely chelating with the metal ions. Subsequently, the mixture was heated at 353 K to evaporate the solvent. The precipitate was then dried in an oven at 393 K for 24 h. Finally, the product was calcined in a furnace under nitrogen atmosphere at 723 K for 2 h with a heating rate of 2 K/min. In order to investigate the effect of the pH value and the chitosan concentration, the pH value was changed to 7 and 8, while the amount of chitosan addition was varied from 0 to 0.6 g. The samples are denoted as CZ*x*–C*y* (*x* = pH value and *y* = amount of chitosan addition in grams).

2.3. Characterization of CuO–ZnO nanocomposites

The combustion characteristic of the dried samples was investigated with a SDT2960 simultaneous DTA–TGA Universal 2000 at a heating rate of 10 °C/min under a flow of nitrogen (80 mL/min). The specific surface area (S_{BET}) of the composites was determined with a Quantachrome Autosorb-1C instrument at −196 °C. X-ray diffraction (XRD) patterns of the composites were done on a diffractometer (Bruker D8 Advance) using Cu-K_α radiation. The measurements were made at room temperature at a range of 20°–90° on 2θ with a step size of 0.05°. The diffraction patterns were analyzed using the Joint Committee on Powder Diffraction Standards (JCPDS). CuO and ZnO crystallite sizes were calculated by means of the Scherrer Equation as shown below:

$$d = \frac{0.89\lambda}{B\cos\theta} \times \frac{180^\circ}{\pi} \quad (1)$$

where d denotes the mean crystallite size, λ is the X-ray wave length (1.54 Å), and B is the full width half maximum (FWHM) of the peak. The surface morphology and surface compositions of the samples were examined with a field emission scanning electron microscopy (FE-SEM: Hitachi-S4700) equipped with energy-dispersive X-ray spectroscopy (EDS). The samples were sputter coated with gold prior to examination.

3. Results and discussion

Fig. 1 shows a thermal behavior of the products synthesized at different chitosan concentrations investigated by TG–DTA measurement. It can be seen that, without the use of chitosan (CZ_7–C_0), there is an endothermic peak and two exothermic peaks appear at 135, 228 and 259 °C, respectively. The endothermic peak with a weight loss of approximately 10% can be attributed to the loss of residual water in the gel. A large weight loss of approximately 52% between 200 and 280 °C is ascribed to the decomposition of nitrate, $Zn(OH)_2$ to ZnO and $Cu(OH)_2$ to CuO. The addition of chitosan to the precursor solution was found to affect the combustion rate of the gel. At low chitosan concentration (CZ_7–$C_{0.3}$), the peak at approximately 139 °C, corresponding to the removal of water in the gel, still exist. However, the first exothermic peak was found to shift its position from 228 to 203 °C with a sudden decrease in weight of approximately 46%, an indication of autocatalytic combustion behavior at which chitosan served as a fuel. The remaining weight loss (14%) occurring in the region of 203–265 °C could be ascribed to incomplete decomposition of nitrate, $Zn(OH)_2$ to ZnO and $Cu(OH)_2$ to CuO. At a higher chitosan concentration (CZ_7–$C_{0.6}$), the decomposition of the gel occurred suddenly in a single step, which is potentially due to a greater amount of energy released from the reaction as the increase of fuel. However, the maximum of the exothermic peak was found to slightly shift towards a higher temperature (209 °C) when compared to that of the sample CZ_7–$C_{0.3}$. This observation could be due to the entrapment of chitosan molecules surrounded by metal hydroxides, which interrupt the role of chitosan. The similar trends

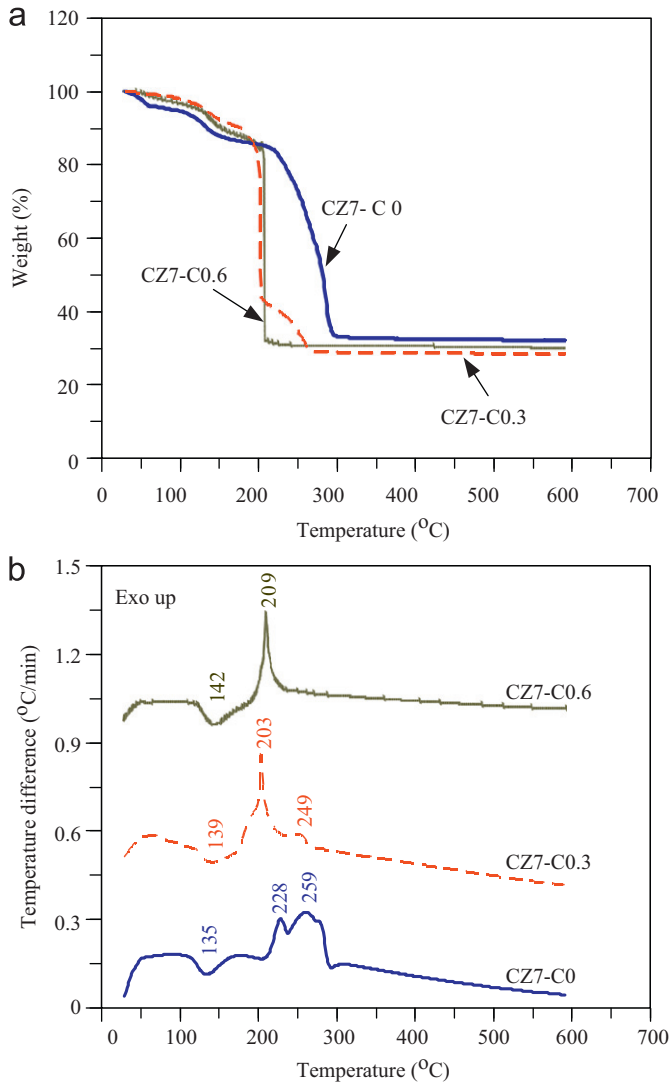

Fig. 1. TG (a) and DTA (b) curves of the dried gel prepared without (CZ_7–C_0) and with chitosan (CZ_7–$C_{0.3}$ and CZ_7–$C_{0.6}$).

were also observed for the samples synthesized at other pH values (not shown here).

The apparent morphologies of the samples synthesized at different pH values and chitosan concentrations examined by means of a SEM are shown in Fig. 2. The surface compositions (Cu/Zn) were investigated by SEM–EDX with several spots and the average value was considered for each system. The results of Cu/Zn ratio of all samples are summarized in Table 1. The samples synthesized without the use of chitosan were found to have two different morphologies (Fig. 2a–c). At pH 6 (Fig. 2a), the sample shows a platelet-like morphology and a pyramid-shaped structure with average size of approximately 1 and 3 μm, respectively. The Cu/Zn ratio of the platelet and the pyramid was found to be 2.53 (circle) and 0.09 (rectangular), respectively, an indication for the separate formation of CuO and ZnO phases since the initial ratio of Cu/Zn was equal to 1. The similar trends were also observed when the pH value was increased to 7 (Fig. 2b) and 8 (Fig. 2c).

Once chitosan was applied at low concentration (Fig. 2d–f), the platelet-like morphology and the pyramid-shaped structure were no longer observed and instead only an aggregation of irregular spherical structure was obtained. The Cu/Zn ratio was found to be 0.88, 0.92 and 1.04 for the samples synthesized at pH 6, 7 and 8, respectively, which was indicative of a homogeneous mixture of CuO and ZnO nanoparticles. The increase of chitosan concentration was found to change the irregular spherical structure to a foamy filament and spongy in nature for the samples synthesized at pH 6 and 7 (Fig. 2g and h). This could be due to the fact that the addition of chitosan in reaction mixture acts as a fuel as evident from the thermal analysis data. The increase in chitosan content acts as a space filling agent, which possibly leaves empty spaces during the combustion process and thus resulting in the existence of huge porosity of the CuO–ZnO nanocomposites. At pH 8 (Fig. 2i), a denser aggregation of irregular spherical structure was obtained. The Cu/Zn ratio was found to be 0.72, 0.75 and 0.80 for the samples synthesized at pH 6, 7 and 8, respectively. Note that these ratios were considerably lower than unity, indicating that the large portion of the external surface of the particles were coated by zinc oxides.

The XRD patterns of the samples synthesized at different pH values and chitosan concentrations are shown in Fig. 3. The peaks at 32.54°, 35.52°, 38.81°, 48.56° and 61.50° of the 2θ were attributed to the CuO diffractions of (110), (002), (111), (202) and (113), respectively. The other diffraction peaks matched the standard data for a heaxagonal wurtzite ZnO (JCPDS 36–1451). The peak intensities of the samples synthesized without the use of chitosan were found to be decreased with increasing the pH of the mixture (Fig. 3a–c), which is attributed to the decrease in crystallinity. The average crystallite sizes of the samples calculated with the Scherrer Equation on the CuO (111) and the ZnO (100) are listed in Table 1. The average crystallite size of CuO was found to be 28.5, 18.2 and 17.8, while that of ZnO was found to be 36.8, 28.9 and 28.5 for the samples synthesized at pH 6, 7 and 8, respectively.

The XRD pattern (Fig. 3a–c) of the samples synthesized with chitosan appeared at the identical 2θ angles as that of the samples synthesized without chitosan, indicating that chitosan did not alter the crystalline phases of the samples. At low chitosan concentration, the CuO and ZnO crystallite sizes were found to be considerably smaller than those of the samples prepared without the use of chitosan. However, further increase in the chitosan concentration resulted in a significant increase in crystallite sizes of CuO and ZnO.

The variation in CuO and ZnO crystallite sizes and their morphologies could be attributed to the interaction between chitosan molecules and metal cations. Under near neutral conditions (pH 6–8), nitrogen atoms of amino groups along the backbone chains of chitosan molecules

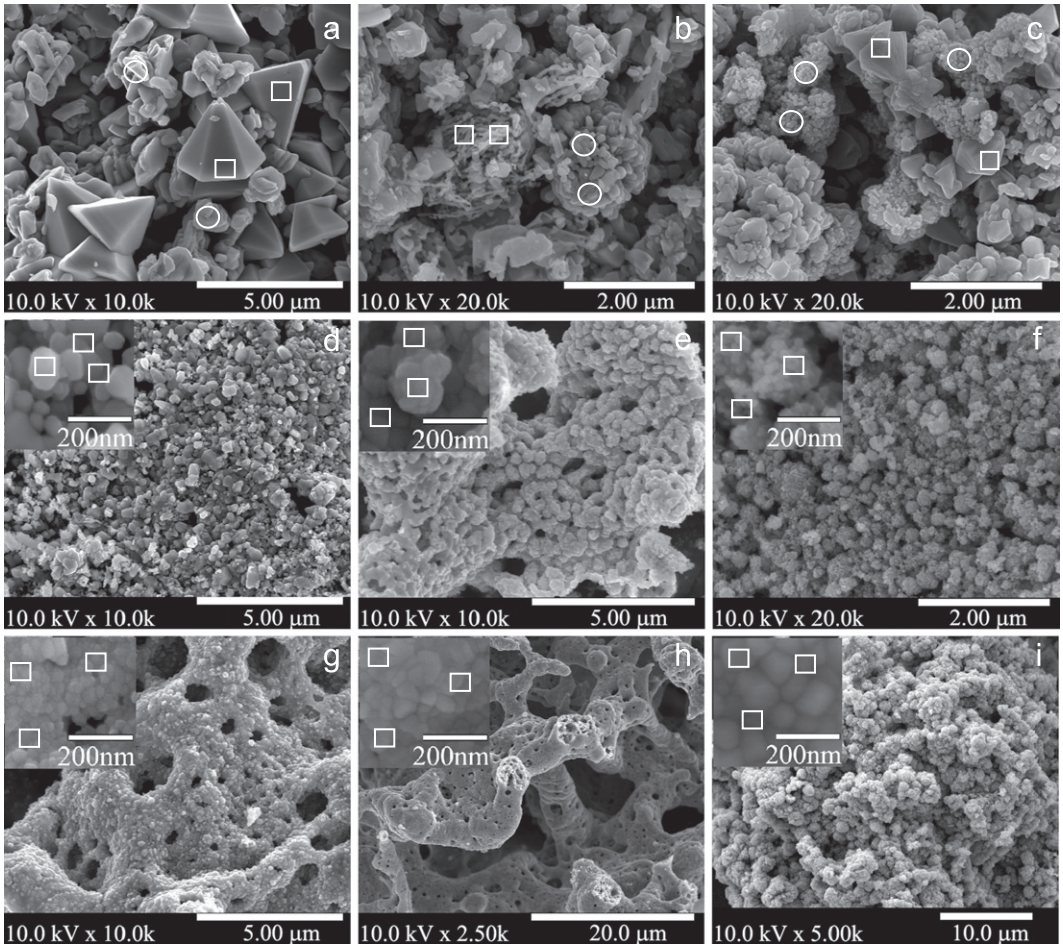

Fig. 2. SEM images of CZ_6–C_0 (a), CZ_7–C_0 (b), CZ_8–C_0 (c), CZ_6–$C_{0.3}$ (d), CZ_7–$C_{0.3}$ (e), CZ_8–$C_{0.3}$ (f), CZ_6–$C_{0.6}$ (g), CZ_7–$C_{0.6}$ (h) and CZ_8–$C_{0.6}$ (i).

Table 1
Surface compositions reported as average value, metal oxides crystallite size and BET surface area.

Catalysts[a]	Position	Cu/Zn	Metal oxides crystallite size (nm)		BET surface area (m^2/g)
			CuO	ZnO	
CZ_6–C_0	rectangular	0.09	28.5	36.8	2.0
	circle	2.53			
CZ_6–$C_{0.3}$	rectangular	0.88	13.4	30.6	28.6
CZ_6–$C_{0.6}$	rectangular	0.72	15.1	24.5	18.4
CZ_7–C_0	rectangular	0.27	18.2	28.9	14.0
	circle	4.44			
CZ_7–$C_{0.3}$	rectangular	0.92	13.6	21.6	31.5
CZ_7–$C_{0.6}$	rectangular	0.75	16.3	26.7	21.4
CZ_8–C_0	rectangular	0.16	17.8	28.5	17.2
	circle	1.31			
CZ_8–$C_{0.3}$	rectangular	1.04	11.8	21.8	32.1
CZ_8–$C_{0.6}$	rectangular	0.80	17.0	26.2	17.8

[a]The samples are denoted as CZ*x*–C*y* where *x* is the pH value and *y* is the amount of chitosan addition in grams.

hold free electrons [18,19], which can bind to copper species and zinc species by chelation. This result not only reduce the quantity of available copper species and zinc species as seeding but also prevent further growth in size of their structure since they were limited within the chitosan network. With further increasing the chitosan concentration at a higher pH value, the chitosan amount was beyond the solubility limit, leading to the formation of highly dense chitosan network. Copper species and zinc species hardly penetrated within the voids of chitosan network and randomly adsorbed on the external chitosan network. Therefore, the role of the chitosan molecules to prevent the growth of particles was inefficient when the excessive amount of the chitosan was used.

4. Conclusion

CuO–ZnO nanocomposites were produced by a chitosan-assisted solution combustion method. Chitosan was found to have three main roles on the formation of the CuO–ZnO nanocomposites: (i) chitosan could induce a homogenous mixture of CuO and ZnO nanoparticles, (ii) chitosan could prevent the growth of CuO and ZnO nanoparticles and (iii) chitosan acted as a fuel. This finding indicates that chitosan constitutes a feasible option as an organic additive for the synthesis of CuO–ZnO nanocomposites via the solution combustion method due to its potentially low costs and environmentally benign nature.

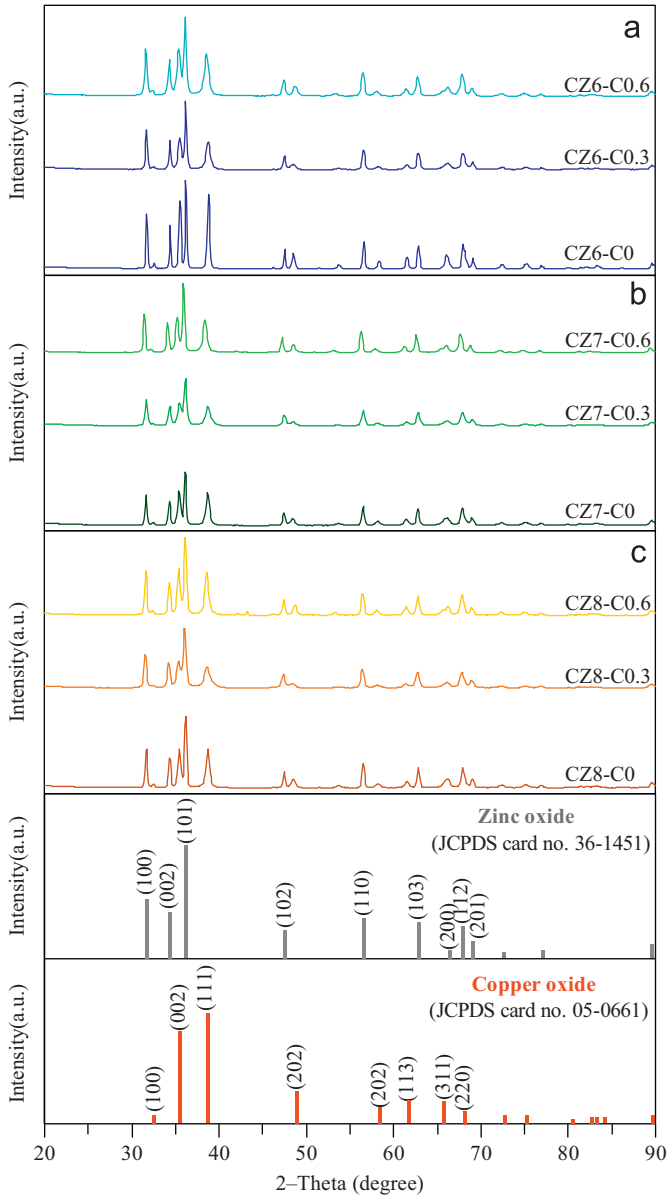

Fig. 3. XRD patterns of the products synthesized at pH 6 (a) pH 7 (b) and pH 8 (c).

Acknowledgments

This work was financially supported by the Research Grant for New Scholar (Grant no. MRG5480196) co-funded by the Thailand Research Fund (TRF); the Commission on Higher Education, Thailand; and Kasetsart University, Thailand. The authors would like to thank the National Center of Excellence for Petroleum, Petrochemical and Advanced Materials (NCE-PPAM), and Kasetsart University Research and Development Institute (KURDI). Support from the "National Research University Project of Thailand (NRU) is also acknowledged.

References

[1] J.P. Greeley, Active site of an industrial catalyst, Science 336 (2012) 810–811.
[2] H. Kidowaki, T. Oku, T. Akiyama, Fabrication and characterization of CuO/ZnO solar cells, Journal of Physics: Conference Series 352 (2012) 012022.
[3] M.-R. Yu, G. Suyambrakasam, R.-J. Wu, M. Chavali, Performance evaluation of ZnO–CuO hetero junction solid state room temperature ethanol sensor, Materials Research Bulletin 47 (2012) 1713–1718.
[4] S.-J. Kim, C.W. Na, I.-S. Hwang, J.-H. Lee, One-pot hydrothermal synthesis of CuO–ZnO composite hollow spheres for selective H_2S detection, Sensors and Actuators B-Chemical 168 (2012) 83–89.
[5] Z. Liu, H. Bai, S. Xu, D.D. Sun, Hierarchical CuO/ZnO "corn-like" architecture for photocatalytic hydrogen generation, International Journal of Hydrogen Energy 36 (2011) 13473–13480.
[6] C. Zhang, L. Yin, L. Zhang, Y. Qi, N. Lun, Preparation and photocatalytic activity of hollow ZnO and ZnO–CuO composite spheres, Materials Letters 67 (2012) 303–307.
[7] R. Raudaskoski, M.V. Niemelä, R.L. Keiski, The effect of ageing time on co-precipitated Cu/ZnO/ZrO_2 catalysts used in methanol synthesis from CO_2 and H_2, Topics in Catalysis 45 (2007) 57–60.
[8] Y. Guo, W. Meyer-Zaika, M. Muhler, S. Vukojević, M. Epple, Cu/Zn/Al xerogels and aerogels prepared by a sol–gel reaction as catalysts for methanol synthesis, European Journal of Inorganic Chemistry 23 (2006) 4774–4781.
[9] X. Guo, D. Mao, G. Lu, S. Wang, G. Wu, Glycine-nitrate combustion synthesis of CuO–ZnO–ZrO_2 catalysts for methanol synthesis from CO_2 hydrogenation, Journal of Catalysis 271 (2010) 178–185.
[10] K. Laishram, R. Mann, N. Malhan, Effect of complexing agents on the powder characteristics and sinterability of neodymium doped yttria nanoparticles, Powder Technology 229 (2012) 148–151.
[11] X. Li, Z. Feng, J. Lu, F. Wang, M. Xue, G. Shao, Synthesis and electrical properties of $Ce_{1-x}Gd_xO_{2-x/2}$ (x=0.05–0.3) solid solutions prepared by a citrate-nitrate combustion method, Ceramics International 38 (2012) 3203–3207.
[12] K. Laishram, R. Mann, N. Malhan, Single step synthesis of yttrium aluminum garnet ($Y_3Al_5O_{12}$) nanopowders by mixed fuel solution combustion approach, Ceramics International 37 (2011) 3743–3746.
[13] W. Wang, X. Liu, F. Gao, C. Tian, Synthesis of nanocrystalline $Ni_1Co_{0.2}Mn_{1.8}O_4$ powders for NTC thermistor by a gel auto-combustion process, Ceramics International 33 (2007) 459–462.
[14] D. Parviz, M. Kazemeini, A.M. Rashidi, Kh.J. Jozani, Synthesis and characterization of MoO_3 nanostructures by solution combustion method employing morphology and size control, Journal of Nanoparticle Research 12 (2010) 1509–1521.
[15] M. Ajmal, A.H. Khan, S. Ahmad, A. Ahmad, Role of sawdust in the removal of copper(II) from industrial wastes, Water Research 32 (1998) 3085–3091.
[16] A. Degen, M. Kosec, Effect of pH and impurities on the surface charge of zinc oxide in aqueous solution, Journal of the European Ceramic Society 20 (2000) 667–673.
[17] J. Berger, M. Reist, J.M. Mayer, O. Felt, N.A. Peppas, R. Gurny, Structure and interactions in covalently and ionically crosslinked chitosan hydrogels for biomedical applications, European Journal of Pharmaceutics and Biopharmaceutics 57 (2004) 19–34.
[18] A.R. Shetty, Master's Thesis: Metal Anion Removal From Wastewater Using Chitosan in a Polymer Enhanced Diafiltration System, Worcester Polytechnic Institute, United States, 2006.
[19] V.K. Mourya, N.N. Inamdar, A. Tiwari, Carboxymethyl chitosan and its applications, Advanced Materials Letters 1 (2010) 11–33.